

Tuning a Josephson junction through a quantum critical point

J. K. Freericks,¹ B. K. Nikolić,¹ and P. Miller²

¹*Department of Physics, Georgetown University, Washington, D.C. 20057-0995*

²*Department of Physics, Brandeis University, Waltham, Massachusetts 02454*

(Received 3 March 2001; published 10 July 2001)

We tune the barrier of a Josephson junction through a zero-temperature metal-insulator transition and study the thermodynamic behavior of the junction in the proximity of the quantum-critical point. We examine a short-coherence-length superconductor and a barrier (that is described by a Falicov-Kimball model) using the local approximation and dynamical mean-field theory. The inhomogeneous system is self-consistently solved by performing a Fourier transformation in the planar momentum and exactly inverting the remaining one-dimensional matrix with the renormalized perturbation expansion. Our results show a delicate interplay between oscillations on the scale of the Fermi wavelength and pair-field correlations on the scale of the coherence length, variations in the current-phase relationship, and dramatic changes in the characteristic voltage as a function of the barrier thickness or correlation strength (which can lead to an “intrinsic” pinhole effect).

DOI: 10.1103/PhysRevB.64.054511

PACS number(s): 74.50.+r, 74.80.-g, 71.27.+a, 71.30.+h

I. INTRODUCTION

The theoretical understanding of Josephson junctions has progressed dramatically over the past four decades.^{1,2} Recent advances³ have been fostered by nanofabrication of superconducting mesoscopic devices,⁴ which, together with high-temperature superconductor junctions, have revived interest in the transport properties of superconductors weakly coupled through a normal region. The interplay between phase-coherent electron propagation in the normal region and macroscopic phase coherence of Cooper pairs in superconductors generates unique quantum interference phenomena since the proximity effect in such systems is mediated by a phase-coherent Andreev reflection.^{5,6} However, little attention has been paid to quantum effects on transport arising from many-body correlations in the barrier separating the superconductors. Such junctions are frequently encountered in high- T_c systems where both superconducting electrodes and the normal region are highly correlated electronic systems.⁷

Low- T_c junctions have large superconducting coherence lengths, and effects on the scale of the Fermi wavelength can usually be averaged over to accurately describe junctions by a quasiclassical (single-particle) approach. As the coherence length of the superconductor becomes smaller and smaller (as in high- T_c junctions) one can no longer ignore the interplay between oscillations brought on by the Fermi surface and those due to pair-field correlations. In addition, as junction sizes are made smaller and smaller, the barrier needs to be tuned close to the metal-insulator transition in order to maintain a large characteristic voltage (where properties of a Josephson junction have been thought to be optimized⁸). The conventional proximity-effect theory cannot account for supercurrent transport in junctions where the barrier approaches a metal-insulator transition.⁷ Therefore, these junctions must be described in a full many-body approach that can properly account for the change in character of the quantum-mechanical system as the correlations drive a metal-insulator transition. The standard single-particle approaches, like the full quantum-transport theories (scattering

formalism^{5,6,9} and Green's-function techniques^{10,11}) or traditional quasiclassical Green's-function methods¹² are inadequate for this purpose (in general, the quasiclassical approaches do not require a quasiparticle assumption,¹³ but the usual quasiclassical Green's function, employed in nonuniform superconductivity problems, can be expanded in terms of Andreev quasiparticle eigenfunctions and energies¹⁴).

Recent progress in the dynamical mean-field theory¹⁵ has shown how to generalize the local approximation to inhomogeneous systems¹⁶ and to Josephson junctions.¹⁷ Here we utilize this formalism to examine what happens as the barrier material is tuned through a quantum-critical transition where the single-particle density of states is suppressed to zero and a correlated metal-insulator transition occurs. The model we choose to describe the barrier is the Falicov-Kimball model¹⁸ that has a metal-insulator transition, but the metallic phase is not a Fermi liquid as it is in a more traditional Hubbard model.¹⁹ The Falicov-Kimball model is chosen because it describes correlation effects due to strong disorder scattering (which is present in many Josephson junctions) and because the dynamical mean-field theory solution does not require quantum Monte Carlo simulation, so it is dramatically easier to analyze than the Hubbard model. The Falicov-Kimball model possesses only charge fluctuations, and thereby ignores all Kondo-like (spin-flip scattering) effects in the barrier of the Josephson junction. We expect results for the Falicov-Kimball model and the Hubbard model to be similar in the insulating phase, but to differ in the metallic phase.

We find that in the vicinity of the metal-insulator transition, it is important to include self-consistency effects and many-body effects. The simple analytical treatments⁵ of Josephson junctions rely on the usage of rigid boundary conditions,² i.e., a step-function model for the pair potential at a normal-superconductor interface. This is justified in narrow junctions (barrier width smaller than the bulk coherence length ξ_0) where the effect of the constriction induced by the narrow barrier on the order parameter of the much wider superconductors is “geometrically diluted,” or in wide junctions with high resistivity barriers (in both cases the critical current of the junction is much smaller than the bulk

critical current of the superconducting leads²⁰). On the other hand, a self-consistent solution for the variation of the order parameter $\Delta(z)$ [i.e., pair-correlation function $F(z) = -\Delta(z)/U(z)$ with $U(z)$ the site-dependent interaction strength] induced by the current flow or geometry, not only ensures current conservation and allows one to find the critical current in an arbitrary geometry,²¹ but is unavoidable in situations where the proximity effect induces appreciable superconductivity in the normal region,²² or when the thickness of the weak link is comparable¹⁰ to ξ_0 . Thus, the microscopic self-consistent calculations¹⁰ reveal a variation of Δ on length scales (like λ_F , the Fermi wavelength) smaller than ξ_0 (which is also of importance in high- T_c junctions where the quasiclassical approximation,¹² $\xi_0 \gg \lambda_F$, does not hold). Our junctions are wide, and even in the tunneling limit (i.e., with a correlated insulator barrier), they require a self-consistent treatment because the many-body effects prevent a description in terms of simple phenomenological parameters (like the barrier transparency). Both self-consistency effects and many-body correlations are automatically included via the dynamical mean-field theory.

Our results should shed light on high- T_c superconductors even though we are restricting ourselves to s -wave symmetry order parameters. This is because the high- T_c superconductors have short coherence lengths (on the order of a few lattice spacings) and have barrier materials [either from grain boundaries, ion damage, or doping (such as Co-doping)] that are correlated and lie close to the Mott metal-insulator transition.⁷ Our examination of s -wave superconductors in this limit illuminates this physical regime without adding the complicated geometrical effects that arise from d -wave order parameters (which will be investigated in a future study).

In Sec. II we briefly describe the formalism that is used in our computational techniques. Section III contains results on tuning through the quantum-critical point by increasing the correlation energy at a fixed barrier thickness. We examine four cases: (i) thin barrier; (ii) bilayer barrier; (iii) barrier on the order of the bulk coherence length; and (iv) thick barrier. In Sec. IV we tune the metal-insulator transition by increasing the thickness of the barrier at fixed correlation energy. We examine a weakly correlated metal barrier, a strongly correlated metal, and a Mott insulator, finding deviations from quasiclassical results for the correlated insulator. Our conclusions are presented in Sec. V.

II. FORMALISM

The computations require a self-consistent calculation of the properties of a Josephson junction within a many-body formalism. To start, we need to have a solution of the bulk superconductor, which will provide the “boundary condition” for the simulations in the bulk boundaries of the junction. The bulk problem can be solved directly in both the absence of a supercurrent and in the presence of a supercurrent (where there is a uniform variation in the phase of the superconducting order parameter). The uniform bulk solution is then employed to provide the boundary conditions for the junction beyond the region where we determine properties self-consistently. The inhomogeneous problem consists of N

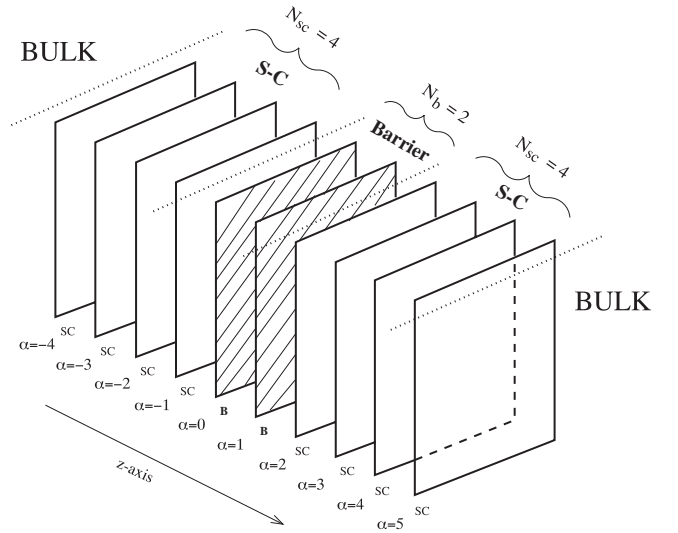


FIG. 1. Microscopic stacked planar geometry of a Josephson junction. The sandwich of $N = 10$ planes; $N_{SC} = 4$ superconducting planes coupled to a bulk superconductor on the left and $N_b = 2$ barrier planes on the right, followed by a further $N_{sc} = 4$ superconducting planes coupled to another bulk superconductor on the right. The junction is allowed to have spatial inhomogeneity only within the N modeled planes, but the calculations are for an infinite system. In our calculations we always take $N_{SC} = 30$ and N_b ranges from 1 to 80.

self-consistent planes embedded in the bulk superconductor on each side (see Fig. 1). The self consistent region consists of a sandwich of N_b barrier planes surrounded by N_{SC} planes on each side $N = N_b + 2N_{SC}$ (the word “barrier” is used since the material through which the weak link between superconductors is made will have its properties tuned from a metal to an insulator). In our solutions we choose $N_{SC} = 30$ and N_b ranges from 1 to 80. Since the coherence length of the superconductor is $\xi_0 = \hbar v_F / (\pi \Delta) \approx 4a$ (with a the lattice spacing) the self-consistent superconducting region is approximately eight times the bulk coherence length, which we find to be sufficient for our calculations. This approach does not require us to make any assumptions about the boundary conditions at the interface between the barrier and the superconductor, since they are determined self-consistently. The approximation is the presence of a (typically small) discontinuity in the supercurrent at the bulk superconductor-self-consistent-superconductor interface. We have found that the superconducting order has always healed to its bulk value at that point, but sometimes there can be a jump of the superconducting phase when one nears the critical current of the junction. This discontinuity in the phase (corresponding to a breakdown of current conservation at the bulk superconductor-simulated superconductor interface) can become large for thick insulating barriers or when one lies on the decreasing-current side of the current-phase diagram (see below).

We simulate an inhomogeneous system of stacked square lattice planes that correspond to the superconductor-barrier-superconductor sandwich of a Josephson junction. A lattice

site corresponds to a unit cell (which we normally picture as being one atomic site), and we assume a tight-binding picture with the same hopping integral t_{ij} between atomic sites within a plane and atomic sites between the planes. This description implies that we are assuming the “bare” kinetic energy of the superconductor and the barrier are identical (note that the renormalized density of states can be very different, especially when the barrier is a correlated insulator). Such a condition is not necessary in this formalism, but we include it for simplicity, since it reduces the number of parameters that are varied in the junction. The superconductor is described by an attractive Hubbard model¹⁹ in the Hartree-Fock approximation. This is equivalent to the conventional (BCS) Bardeen-Cooper-Schrieffer²³ [or more accurately, the Bogoliubov–de Gennes²⁴ (which involves a nonconstant density of states due to the tight-binding approach)] description, except in this case the energy cutoff is determined by the electronic bandwidth rather than the phonon frequency. In fact, the attractive Hubbard model offers richer behavior (that is not employed in this contribution) showing a crossover to preformed pairs. By including higher-order processes in U , through a T matrix²⁵ or a dynamical mean-field theory²⁶ approach, one can study the crossover²⁷ from BCS superconductivity, where pair formation and condensation occur at T_c , to preformed pairs that condense at a lower temperature (this should be important in short-coherence-length superconductors like the high- T_c materials). The barrier is described by a Falicov-Kimball model¹⁸ at half-filling. This model has two kinds of particles: (i) mobile electrons and (ii) static ions. The average concentration of electrons is one per site and the average concentration of ions is one-half per site. When an electron and an ion occupy the same lattice site, there is a Coulomb attraction U_{FK} between them. One can view this system as a binary alloy of A and B ions at 50% concentration with U_{FK} being the difference in site energy between the A and B ionic sites (the off-diagonal energy is assumed to be the same for the A and B ions). The many-body problem is solved by taking an annealed average and is essentially the simplest disorder problem (and the simplest many-body problem). It undergoes a metal-insulator transition in the bulk²⁸ (see below), which is why we adopt it for study here.

The Hamiltonian for the Josephson junction is then

$$H = \sum_{ij\sigma} t_{ij} c_{i\sigma}^\dagger c_{j\sigma} + \sum_i U_i \left(c_{i\uparrow}^\dagger c_{i\uparrow} - \frac{1}{2} \right) \left(c_{i\downarrow}^\dagger c_{i\downarrow} - \frac{1}{2} \right) + \sum_{i\sigma} U_i^{FK} c_{i\sigma}^\dagger c_{i\sigma} \left(w_i - \frac{1}{2} \right), \quad (1)$$

where $c_{i\sigma}^\dagger$ ($c_{i\sigma}$) creates (destroys) an electron of spin σ at site i , t_{ij} is the hopping integral between nearest-neighbor sites i and j (we measure energies in units of t), $U_i = -2$ is the attractive Hubbard interaction for sites within the superconducting planes, U_i^{FK} is the Falicov-Kimball interaction for planes within the barrier, and w_i is a classical variable that equals 1 if an A ion occupies site i and is zero if a B ion occupies site i . A chemical potential μ is employed to determine the filling. Since we work at half-filling for both the

superconductor and the barrier, we have $\mu = 0$. Note that if $U_i = U_i^{FK} = 0$ for all lattice sites, the Hamiltonian describes tight-binding electrons on a simple-cubic lattice.

The superconducting regions are described by an attractive Hubbard model with $U_i = -2$ and $w_i = 0$ for all superconductor sites. The homogeneous bulk superconductor has a transition temperature $T_c = 0.11$ and a zero-temperature order parameter $\Delta = 0.198$. This yields a standard BCS gap ratio $2\Delta/(k_B T_c) \approx 3.6$ and a coherence length $\xi_0 = \hbar v_F / (\pi \Delta)$ that ranges from $3.5a$ to $4.3a$ depending on whether we average the absolute value of v_F over the Fermi surface or take the root-mean-square of v_F (a cubic lattice at half-filling has a direction-dependent Fermi velocity); a fit of the decay of the superconducting order as it is disturbed at the superconductor-barrier interface¹⁷ gives $\xi_0 \approx 3.7a$. The bulk critical current per unit area is $I_{c,\text{bulk}} = 0.0289(2et)/(\hbar a^2)$. The value of our bulk critical current density is slightly higher than the one determined by a Landau depairing velocity $v_d = \Delta/\hbar k_F$ ($j_{c,\text{bulk}} = env_d$, where the density of particles is $n = k_F^3/2\pi^2$, assuming a spherical Fermi surface) because of the possibility to have gapless superconductivity in three dimensions at superfluid velocities slightly exceeding²⁹ v_d (note that k_F is direction dependent for a cubic lattice at half-filling). Calculations on our junction are performed at a temperature of $T = 0.01$, which is effectively at the zero-temperature limit ($T/T_c \approx 0.09$) for the superconducting properties. The barrier region is described by a half-filled Falicov-Kimball model in the symmetric limit of $\langle w_i \rangle = 0.5$. In the bulk, this barrier undergoes a metal-insulator transition at $U_{FK} \approx 4.9$ (since the bandwidth of the simple cubic lattice is 12, the metal-insulator transition occurs when U_{FK} is on the order of one-half of the bandwidth). This is illustrated in Fig. 2(a) where we show the single-particle density of states for a bulk barrier as a function of U_{FK} . The density of states for this model is independent of temperature.²⁸ Since the system is not a Fermi liquid for nonzero U_{FK} , one can see the density of states first develops a pseudogap and then is suppressed entirely to zero as the correlations are increased and it becomes a correlated insulator. The opening of the gap is continuous. In Fig. 2(b) we show the imaginary part of the local self-energy at low energies. This result is also temperature independent.²⁸ We see that the curvature of the self-energy has the wrong sign in the metallic regime (which is one reason why it is not a Fermi liquid) and that it diverges (and becomes a δ function) as the system crosses over into the insulating phase. This occurs because the self-energy develops a pole at zero energy in the insulating phase. Such behavior can only be seen in a many-body treatment of the system.

The inhomogeneous system is solved by employing the matrix formulation of Nambu³⁰ for the Green's function $G(\mathbf{r}_i, \mathbf{r}_j, i\omega_n)$ for two lattice sites \mathbf{r}_i and \mathbf{r}_j at the Matsubara frequency $i\omega_n = i\pi T(2n+1)$,

$$G(\mathbf{r}_i, \mathbf{r}_j, i\omega_n) = \begin{pmatrix} G(\mathbf{r}_i, \mathbf{r}_j, i\omega_n) & F(\mathbf{r}_i, \mathbf{r}_j, i\omega_n) \\ \bar{F}(\mathbf{r}_i, \mathbf{r}_j, i\omega_n) & -G^*(\mathbf{r}_i, \mathbf{r}_j, i\omega_n) \end{pmatrix}, \quad (2)$$

and the corresponding local self-energy,

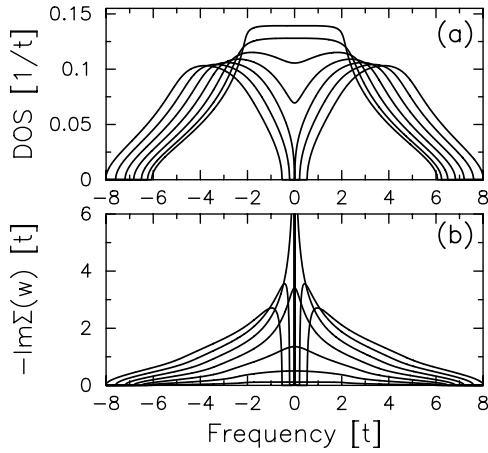


FIG. 2. (a) Electronic density of states for the bulk barrier (simple-cubic lattice) described by the Falicov-Kimball model in the local approximation. The value of U_{FK} ranges from 1 to 7 in steps of 1. As U_{FK} increases, the density of states first develops a pseudogap and then a real gap. (b) Absolute value of the imaginary part of the local retarded self-energy for low frequency on the real axis. See how the curvature has the wrong sign for a Fermi liquid and how the imaginary part diverges at zero frequency as one goes through the quantum-critical point and a pole develops in the self-energy.

$$\Sigma(\mathbf{r}_i, i\omega_n) = \begin{pmatrix} \Sigma(\mathbf{r}_i, i\omega_n) & \phi(\mathbf{r}_i, i\omega_n) \\ \phi^*(\mathbf{r}_i, i\omega_n) & -\Sigma^*(\mathbf{r}_i, i\omega_n) \end{pmatrix}. \quad (3)$$

The diagonal and off-diagonal Green's functions are defined, respectively, as

$$G(\mathbf{r}_i, \mathbf{r}_j, i\omega_n) = - \int_0^\beta d\tau \exp(i\omega_n \tau) \langle T_\tau \hat{c}_{j\sigma}(\tau) \hat{c}_{i\sigma}^\dagger(0) \rangle, \quad (4)$$

$$F(\mathbf{r}_i, \mathbf{r}_j, i\omega_n) = - \int_0^\beta d\tau \exp(i\omega_n \tau) \langle T_\tau \hat{c}_{j\uparrow}(\tau) \hat{c}_{i\downarrow}(0) \rangle, \quad (5)$$

where T_τ denotes time ordering in τ and $\beta = 1/T$.

The self-energies and Green's functions are coupled together through Dyson's equation,

$$\begin{aligned} G(\mathbf{r}_i, \mathbf{r}_j, i\omega_n) &= G^0(\mathbf{r}_i, \mathbf{r}_j, i\omega_n) \\ &+ \sum_l G^0(\mathbf{r}_i, \mathbf{r}_l, i\omega_n) \Sigma(\mathbf{r}_l, i\omega_n) \\ &\times G(\mathbf{r}_l, \mathbf{r}_j, i\omega_n), \end{aligned} \quad (6)$$

where we have included the local approximation for the self-energy, $\Sigma(\mathbf{r}_i, \mathbf{r}_j, i\omega_n) = \Sigma(\mathbf{r}_i, i\omega_n) \delta_{ij}$. The noninteracting Green's function, $G^0(\mathbf{r}_i, \mathbf{r}_j, i\omega_n)$ is diagonal in Nambu space, with upper diagonal component given by

$$G^0(\mathbf{r}_i, \mathbf{r}_j, i\omega_n) = \int d^3\mathbf{k} \frac{e^{i\mathbf{k} \cdot (\mathbf{r}_i - \mathbf{r}_j)}}{i\omega_n + \mu - \epsilon_{\mathbf{k}}}. \quad (7)$$

We emphasize that G^0 is the noninteracting Green's function and is *not* the effective medium of an equivalent atomic problem.

Details of the computational scheme have been described elsewhere.¹⁷ Here we simply summarize the algorithm. The junction is inhomogeneous in the z direction only, since it has translational symmetry within each plane. The algorithm begins by converting the three-dimensional system to a quasi-one-dimensional system using the method of Potthoff and Nolting.¹⁶ We perform a Fourier transformation within each plane to determine the mixed-basis Green's function [defined in terms of two-dimensional momenta (k_x and k_y) and the z -coordinate of the plane] under the assumption that the electronic self-energy is local (but can vary from plane to plane). For each momentum in the two-dimensional Brillouin zone, we have a one-dimensional problem with a sparse matrix, since the only coupling between planes is due to the hopping to each neighboring plane. The infinite "tridiagonal" matrix can be inverted by employing the renormalized perturbation expansion,³¹ which calculates both the single plane and the nearest-neighbor Green's functions. A final summation over the two-dimensional momenta produces the local Green's function and the Green's function for propagation from one plane to its neighboring plane. The dynamical mean-field theory is then employed to calculate the local self-energy from the local Green's function and then the local Green's function is calculated from inverting the quasi-one-dimensional matrix. These two steps are repeated until the Green's functions have converged to a fixed point. At the fixed point, we have a self-consistent solution of the inhomogeneous problem that allows for nonuniform variations in both the pair-field correlations (or equivalently the superconducting order parameter) and in the phase. One important consistency check is total current conservation at each plane in the self-consistent region. All calculations conserve current except in extreme cases for thick insulating barriers (see below). But there can be discontinuities in the current at the bulk-superconductor-self-consistent superconductor interface (since this is far from the Josephson junction, it has a negligible effect on the results). This computational algorithm is a generalization of the conventional Bogoliubov-de Gennes approach to allow for correlations within the barrier.

This algorithm can be performed for the normal state or for the superconducting state and can be performed on the imaginary or real frequency axes. We work on the real axis in order to calculate the normal-state resistance. Since we have a many-body system, we must use Kubo's formula for the conductivity. Details for this calculation appeared elsewhere.¹⁷ Our formalism calculates the conductivity by neglecting vertex corrections and evaluating the simple bubble diagram (which becomes exact in the infinite-dimensional limit³²).

III. TUNING THE CORRELATION STRENGTH THROUGH A METAL-INSULATOR TRANSITION

We begin by presenting results for a fixed barrier thickness, and vary the Falicov-Kimball coupling strength. We

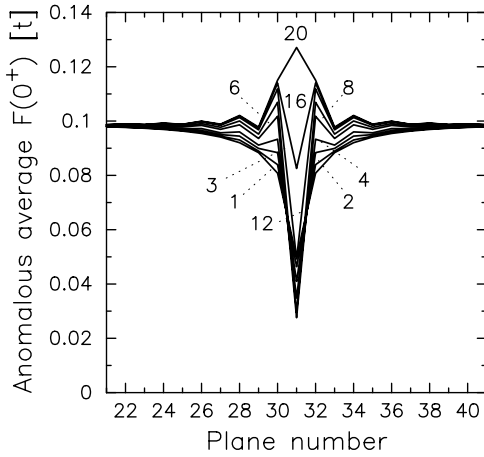


FIG. 3. Proximity effect for a thin barrier ($N_b=1$). The anomalous average is plotted versus plane number (the insulating barrier lies at plane 31). The numbers indicate the value of U_{FK} (1, 2, 3, 4, 6, 8, 12, 16, and 20); the anomalous average monotonically increases with U_{FK} in the range between planes 29 and 30. Note how oscillations develop as the correlations increase until the superconductivity ultimately becomes *enhanced* in the barrier for the strong insulator.

study four different systems: (i) a thin barrier with $N_b=1$; (ii) a bilayer barrier with $N_b=2$; (iii) a barrier on the order of the bulk superconducting coherence length $N_b=5$; and (iv) a thick barrier $N_b=20$.

A. Thin barrier ($N_b=1$)

A single-plane barrier must be in the very strong insulating limit before it can severely affect the transport perpendicular to the plane. Hence we expect to have to increase the Falicov-Kimball interaction to be much larger than 5 before the junction starts to display “insulating” behavior. Similarly, we expect the critical current to be close to the bulk critical current, because the plane is so thin (at least for metallic barriers). In this regime, self-consistency is critical in determining the properties of the junction.²⁰

We begin by examining the proximity effect within the junction. Since the Hubbard attraction is zero within the barrier, the superconducting gap Δ , which is proportional to the Hubbard attraction, identically vanishes there. But we can still examine the superconducting pair-field correlations by plotting the anomalous average at equal times $F(\tau=0^+)$. This Green’s function is continuous as one passes through the superconductor-barrier interface. We show $F(0^+)$ in Fig. 3. Notice how the correlated metal ($U_{FK}<2.5$) appears just as we expect it to: the superconductivity is smoothly depressed as we approach the barrier and then decreases within the barrier as correlations increase. As the bulk barrier enters the pseudogap regime ($2.5<U_{FK}<5$) we see small oscillations appear in the superconductor, and the superconductivity continues to be depressed within the barrier. In the correlated insulator regime ($5<U_{FK}<8$) the oscillations continue to grow and the superconductivity within the barrier is small, but rather insensitive to U_{FK} . In the strong insulating regime ($U_{FK}>8$), we find that the oscillations become large and the

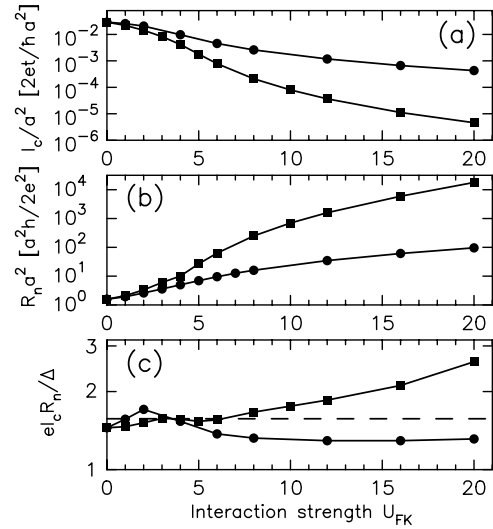


FIG. 4. (a) Critical current, (b) normal-state resistance, and (c) characteristic voltage of the Josephson junctions as a function of the Falicov-Kimball interaction within the barrier. The circular symbols are for $N_b=1$ and the squares are for $N_b=2$. Note how the critical current decreases and the junction resistance increases as expected, and how the characteristic voltage does not depend too strongly on the correlation strength. The dependence on correlation strength for the bilayer junction is much stronger than for the thin junction. The dashed line in (c) is the Ambegaokar-Baratoff prediction.

superconductivity eventually becomes *enhanced within the barrier*. We believe that the oscillations and this enhancement of the anomalous average are arising from a surface effect of the superconducting half planes—each half plane develops oscillations near the surface (as the barrier becomes more insulating).

We show a plot of the Josephson critical current, the normal-state resistance R_n , and the characteristic voltage $I_c R_n$ for the single-plane barrier. The plots are on a semilogarithmic scale. The critical current drops by about two orders of magnitude as U_{FK} increases from 0 to 20. This occurs even though the anomalous average increases in the strongly insulating limit. The plot of R_n shows the expected increase as the correlations increase. But even at a large value of $U_{FK}=20$, the resistance only increases by about two orders of magnitude over the noninteracting limit. Finally, we show the characteristic voltage $I_c R_n$ in Fig. 4(c). Its value does not change much, but shows a mild optimization for the moderately correlated metallic phase. In the metallic limit $U \rightarrow 0$, the $I_c R_n$ product approaches the product of the bulk critical current times the Sharvin resistance, which is $0.287t/e = 1.45\Delta/e$. This result is different from the clean Kulik-Omelyanchuk limit³³ of $\pi\Delta/e$ because we are treating a different geometry from a point contact (which can be described as a “plane” contact). As the correlations increase within the metallic phase, the characteristic voltage peaks for $U_{FK} \approx 2$ at a value somewhat smaller than the dirty limit of the Kulik-Omelyanchuk formula³³ for a superconducting point contact $I_c R_n = 0.66\pi\Delta/e$ at $T=0$. In fact, there are two possibilities for the $I_c R_n$ product of a short contact with diffusive scattering. Namely, in the single-particle picture scat-

tering properties of a normal region can be described by the universal distribution of transparencies D (defined as the distribution of eigenvalues of the matrix $\mathbf{t}\mathbf{t}^\dagger$, where \mathbf{t} is the transmission matrix connecting incoming to outgoing transverse propagating modes⁵) given by either the Dorokhov expression³⁴ $P_{\text{Do}}(D) = (G/2G_Q)[D\sqrt{1-D}]^{-1}$ (valid for most bulk conductors), or the Schep-Bauer distribution³⁵ $P_{\text{SB}}(D) = (G/\pi G_Q)[D^{3/2}\sqrt{1-D}]^{-1}$ (valid for subnanometer-thick barriers³⁶). Here, $G_Q = 2e^2/h$ is the conductance quantum and $G = \int_0^1 dD P(D)D$ is the disorder-averaged conductance. The total current is found by integrating the current carried by a single channel $I(D)$ (with a transparency of D) over the distribution function $P(D)$ as shown in the multiple Andreev reflection theory.⁹ This integral, $I = \int_0^1 dD P(D)I(D)$, then leads to the following characteristic voltages: $I_c R_n = 0.66\pi\Delta/e$ for $P_{\text{Do}}(D)$ and $I_c R_n = 0.61\pi\Delta/e$ for $P_{\text{SB}}(D)$. We find that in the case of a single-plane barrier made of an FK correlated metal, the largest $I_c R_n$ (obtained for $U_{FK} = 2$) is slightly below the value determined by $P_{\text{SB}}(D)$. This can be attributed to effects of self-consistency and the “inverse” proximity effect, or to the fact that such an interface cannot be described by the Schep-Bauer distribution $P_{\text{SB}}(D)$.

As the junction barrier becomes more insulating, the characteristic voltage becomes essentially constant as expected from the Ambegaokar-Baratoff limit³⁷ $\pi\Delta/(2e)$ (dashed line). But the magnitude of the characteristic voltage is approximately 15% smaller than that predicted by them [$\pi\Delta/(2e)$] versus our calculated result of $1.31\Delta/e$. Once again, this small reduction arises from the self-consistency and from the (nonspherical) Fermi-surface averaging of the transport.

B. Bilayer ($N_b = 2$)

We see similar behavior in the bilayer junctions with $N_b = 2$. The correlation strength needed to make an insulating barrier is smaller here, because the barrier is thicker. In Fig. 5, we plot the anomalous average as a function of the plane number. The planes numbered 31 and 32 are where the barrier lies. The behavior is like that seen in the thin barrier case—the correlated metal ($U_{FK} < 2.5$) and pseudogap regions ($2.5 < U_{FK} < 5$) are similar. The correlated insulator regime, where the oscillations in the anomalous average increase, but its value within the barrier is rather insensitive to U_{FK} ($5 < U_{FK} < 7$) and the strong insulating regime ($U_{FK} > 7$) shows an enhancement of the anomalous average within the barrier at an even larger value of U_{FK} (starting at $U_{FK} \approx 14$).

In Fig. 6, we show (a) the current versus phase and (b) the renormalized current-phase relation. As the barrier becomes more insulating, we recover the expected result that $I(\theta) = I_c \sin \theta$ because all of the phase difference takes place over the barrier (in general, the majority of the phase difference occurs over the central plane of the barrier). More metallic barriers have the maximum in the $I(\theta)$ curve pushed to values of θ less than $\pi/2$ as expected due to the self-consistency and the proximity to the bulk critical current.

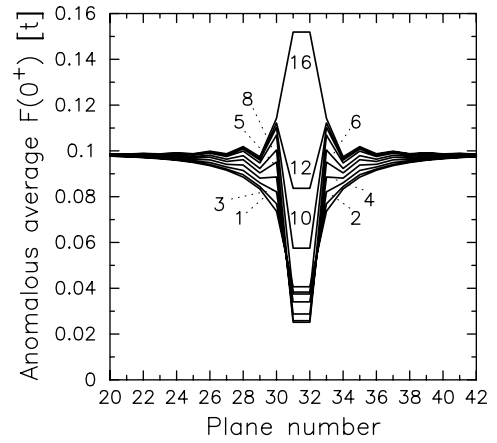


FIG. 5. Anomalous average for differing correlation strengths and $N_b = 2$. Note how similar these results are to the thin barrier case—how the anomalous average initially drops within the barrier, then oscillations develop, followed by an enhancement for the strongest correlation strengths.

The critical current, normal-state resistance, and characteristic voltage appear in Fig. 4. The critical current decreases much more rapidly for the bilayer than for the single-layer junction. The normal-state resistance increases more rapidly as well, since the bilayer has a resistance that is much more than two times the $N_b = 1$ resistance in the strongly insulating limit. The characteristic voltage is quite interesting, because it has nonmonotonic behavior. There is a weak maximum for the moderately correlated metal (near $U_{FK} = 3$), but in the insulating region the voltage increases linearly with the correlation strength, attaining values 40% higher than the Ambegaokar-Baratoff limit. This is quite different from what we expect—a constant characteristic voltage—and the characteristic voltage shows no sign of saturating even at a correlation energy of $U_{FK} = 20$. Of course, the I - V characteristic must become hysteretic once U_{FK} is large enough.

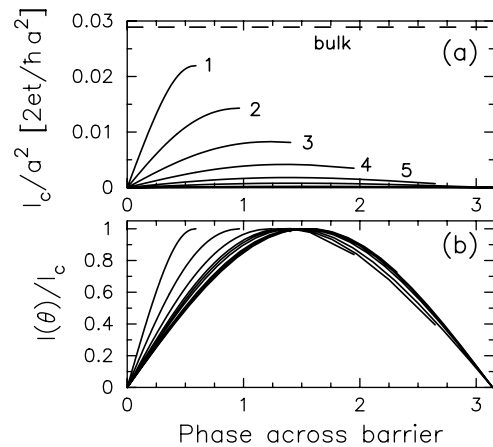


FIG. 6. Current-phase relations for $N_b = 2$. (a) Current-phase relation. Values of U_{FK} include 1, 2, 3, 4, 5, 6, 8, 10, 12, and 16 (labels included for some of the curves). (b) Normalized current-phase relation. Note how the expected sinusoidal dependence enters for insulating barriers.

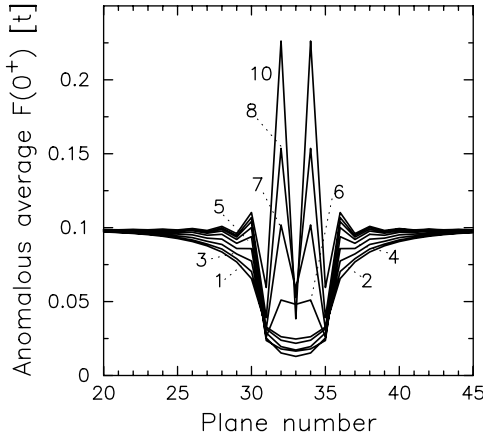


FIG. 7. Anomalous average plotted versus plane number for the $N_b=5$ junction. The values of U_{FK} chosen are 1, 2, 3, 4, 5, 6, 7, 8, and 10. Note how the large oscillations are now separated from each other and are clearly tied to the superconductor-barrier interface.

C. Moderately thick barrier ($N_b=5$)

The barrier region (with $N_b=5$) is chosen to be slightly thicker than the bulk coherence length $\xi_0 \approx 4a$. Here we examine properties of a junction outside of the regime of most analytic approximations. In Fig. 7, we plot the anomalous average versus plane number (the barrier lies at planes numbered 31 to 35). These results are similar to those seen before. In the weak correlation regime ($U_{FK} < 2.5$), the anomalous average is a smooth function that decreases as the correlations increase. Oscillations begin to develop for $2.5 < U_{FK} < 4.5$, but the anomalous average continues to decrease within the barrier. As the correlations increase further, $U_{FK} > 5$, the anomalous average first increases at the center of the barrier, then a two-peak structure emerges, which has a large amplitude oscillation and a minimum at the central plane of the barrier. We can see clearly here that the oscillatory behavior seen in the previous cases is arising from effects occurring at the superconductor-barrier interface as the barrier is tuned through the quantum-critical point (this is further confirmed with the $N_b=20$ data below).

The current-phase relation is similar to that seen for the bilayer, and will not be shown here. The normalized current-phase relation, is plotted in Fig. 8. This result is quite inter-

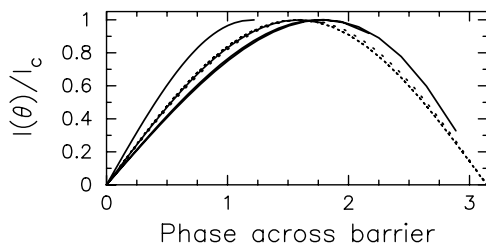


FIG. 8. Normalized current-phase relation. Note how the maximum lies at an angle less than $\pi/2$ for $U_{FK}=1,2$, increases to a value larger than $\pi/2$ for moderate correlations $U_{FK}=3,4$ and then settles down to $\pi/2$ for larger correlations $U_{FK} > 5$ (curves with a dotted line).

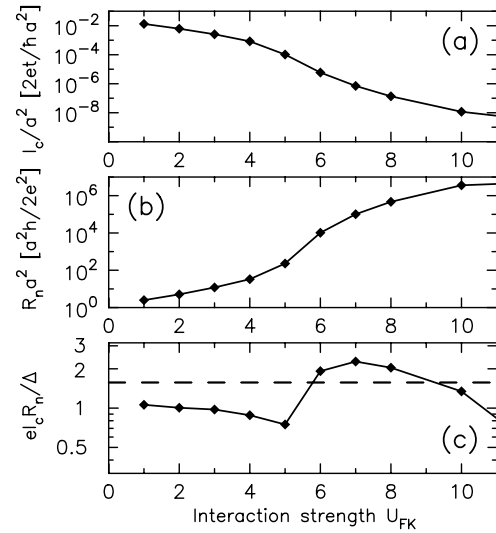


FIG. 9. (a) Critical current, (b) normal-state resistance, and (c) characteristic voltage of the $N_b=5$ (diamond) junction. The metal-insulator transition can be seen in the critical current (a) and (more easily) in the resistance (b), as the regions where the slope of the curves changes most dramatically. In the strongly correlated insulating regime, we find the exponential decay of the current (and increase of the resistance) has a different slope than in the correlated metal regime. The characteristic voltage (c) has complex behavior: it first decreases in the metallic regime, then has a sharp increase at the metal-insulator transition, followed by a decrease as the correlations increase further (the Ambegaokar-Baratoff prediction is the dashed line). Note how the characteristic voltage is maximized just on the insulating side of the metal-insulator transition, and how the maximal value is about 40% larger than the Ambegaokar-Baratoff prediction.

esting. In the weakly correlated regime $U_{FK} < 2.5$, the maximum of the current-phase relation occurs at a phase smaller than $\pi/2$ as expected for a thin metallic barrier. As the correlations increase, the maximum first overshoots $\pi/2$ ($U_{FK}=3,4$), and then returns to its expected location at $\pi/2$ for $U_{FK} > 5$. There is a delicate interplay between the strength of the correlations and the location of the maximum of the current-phase relation.

The critical current, normal-state resistance, and characteristic voltage are plotted in Fig. 9 for $N_b=5$ (diamond). It is difficult to locate the metal-insulator transition from the $N_b=5$ critical current data (except by focusing on the inflection point), but the transition is clearer in the resistance, which has a sharp increase in the range from $U_{FK}=5$ to 6. The characteristic voltage has striking behavior. Starting at a value about 20% less than the Ambegaokar-Baratoff limit in the metallic regime, the voltage initially decreases with correlation strength, then has a sharp increase (by over 100%) at the metal-insulator transition, reaching a maximum almost 40% higher than the Ambegaokar-Baratoff result, until it finally starts to decrease as correlations increase further, continuing to decrease at the largest value of correlations where we performed calculations. Hence, junctions in this regime do see an enhancement of the characteristic voltage on the insulating side of the metal-insulator transition. The behavior is quite complex.

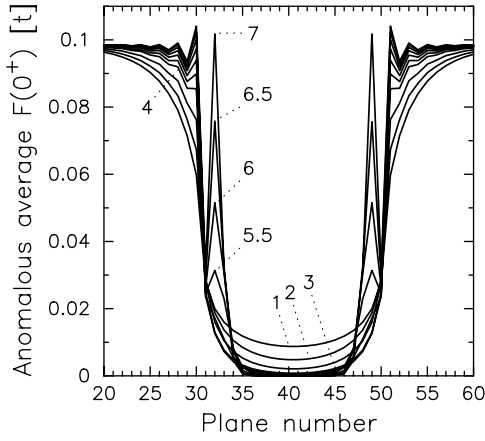


FIG. 10. Anomalous average for a thick junction $N_b=20$. Values of U_{FK} included are 1, 2, 3, 4, 4.5, 5, 5.5, 6, 6.5, and 7. Note how the metallic regime behaves as expected, but oscillations develop in the insulating regime that become huge just inside the barrier.

D. Thick barrier ($N_b=20$)

The thick-barrier junction $N_b=20$ behaves in many respects like the bulk barrier material. The transition from a metal to an insulator occurs at approximately $U_{FK}=5$ as in the bulk, and the junction rapidly develops oscillations in the anomalous average at $U_{FK}\approx 4$. This is shown in Fig. 10. Note how the correlated metal regime behaves entirely as expected—the anomalous average decreases as one approaches and then enters the barrier, but it never gets too small in the metallic regime because of the proximity effect. As the correlations increase, oscillations first develop in the superconductor and then move into the interfacial region, penetrating about one coherence length into the barrier before they are rapidly suppressed within the barrier. We see the same phenomenon as in the thinner junctions: in the insulating regime, the anomalous average can increase to above its bulk value within the barrier, but only close to the superconductor-insulator interface. As the correlations increase, the peak of the anomalous average grows.

The current-phase relation is essentially sinusoidal in these junctions. For the weakly correlated metals, the peak of the $I(\theta)$ curve occurs just above $\pi/2$, but as it becomes more insulating, the peak moves downward toward $\pi/2$ and the current-phase relation becomes $I(\theta)=I_c \sin \theta$, as expected. There is a computational difficulty that enters when we are in the strong-insulator regime for a thick-barrier junction. Here the critical current gets exponentially small, and the computational algorithm loses current conservation through the entire junction (when the calculation is halted at a self-consistency error of one part in 10^7 for the anomalous average at $\tau=0$). Instead, we see an exponential decrease of the current from the value fixed at the bulk superconductor to the value within the barrier. The current is constant within the barrier itself, and the current-phase relation is a nice sine curve, so we believe that the critical current found from our algorithm is accurate, even though, the boundary conditions with the bulk are trying to force more current through the junction than it can have; i.e., the current discontinuity oc-

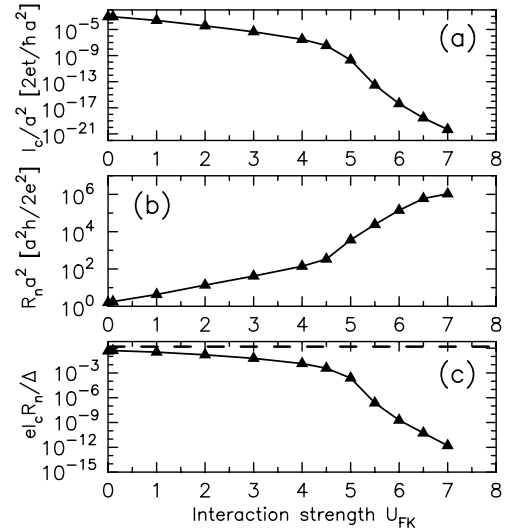


FIG. 11. (a) Critical current, (b) normal-state resistance, and (c) characteristic voltage of the $N_b=20$ (triangle) junctions. Note how the thick junction behaves much like the bulk material. The metal-insulator transition can be clearly seen in the critical current and in the resistance, as the regions where the slope of the curves changes most dramatically. In the strongly correlated insulating regime, we find the exponential decay of the current (and increase of the resistance) has a different slope than in the correlated metal regime. Note that the thick barrier has a sharply suppressed characteristic voltage because the decrease in I_c is much sharper than the increase in R_n . We believe this occurs because the temperature dependence of the resistance is strong, even at these low temperatures. The dashed line is the Ambegaokar-Baratoff prediction.

curs far from the barrier region. This scenario is similar to that of Josephson's original analytic scheme,¹ since in his case, there is no phase gradient over the superconductors, so they carry no current, but there is current in the barrier, since there is a phase difference across it.

The critical current, normal-state resistance, and characteristic voltage appear in Fig. 11. One can see the metal-insulator transition clearly in the I_c curve. Within the metal, the critical current has an exponential dependence on U_{FK} , within the insulator it has a different exponential dependence. In the transition region, it decreases most sharply. We believe the reduction in the rate of decrease in the critical current as U_{FK} is increased into the correlated insulator regime arises in part from the fact that the effective junction thickness is thinner than the true junction thickness due to the oscillations in the anomalous average that develop within the barrier region. The resistance shows the expected behavior as well. One can clearly see the metal-insulator transition as the region where the conductivity changes its functional dependence sharply. Note, however, that the characteristic voltage is severely affected by the metal-insulator transition, since the decrease in the critical current far outweighs the increase in resistance, and the characteristic voltage decreases by many orders of magnitude as one enters the strongly correlated insulator. One reason why this occurs is because the resistance for the correlated insulator depends strongly on temperature. As $T\rightarrow 0$, the resistance becomes very large, but it can be sharply reduced as the temperature

increases. Hence, even though the critical current is at the zero-temperature limit for $T/T_c=0.1$, the resistance still has strong temperature dependence in this regime, which causes the characteristic voltage to be sharply suppressed. Perhaps this behavior plays a role in some junctions that appear to work well at low temperatures, but then fail as the temperature is increased, because on the insulating side of the metal-insulator transition, the resistance has strong temperature dependence.

E. Summary of tuning the correlation energy

We have discovered a number of interesting features of Josephson junctions for short-coherence-length superconductors that have their barrier tuned through the quantum-critical point of a metal-insulator transition. The most striking feature we find is that in the insulating regime, there are oscillations with a wavelength on the order of the Fermi wavelength, that appear at the superconductor-barrier interface and decay on the order of the coherence length on either side of the interface. They can have very large amplitudes (on the order of the bulk value of the anomalous average) within the barrier. We believe that these oscillations are occurring from a “surface” effect intrinsic to the superconductor, and depending on how close the two interfaces are (determined by the thickness of the barrier) they are either independent of each other or can interfere. Note that these results differ from those found in metallic junctions with “geometrically diluted” barriers.¹⁰ There, oscillatory behavior was seen even for metallic barriers $U_{FK}=0$, and the decay length was much longer, leading to a number of cycles before the oscillations are damped. We also found interesting results for the current-phase relations. As expected, thin junctions typically have I_c occur at a phase difference smaller than $\pi/2$, but in all but the single-plane junction, as the correlations increase, the maximal I_c occurs at $\pi/2$ and the curve becomes sinusoidal. For thick barriers, we find the maximum occurs larger than, but close to $\pi/2$ for metallic barriers and then migrates towards $\pi/2$ as the barrier becomes more insulating. Finally, we found a different behavior in the characteristic voltage of a junction. The characteristic voltage is limited in the metallic regime by the bulk critical current of the superconductor multiplied by the junction resistance for a clean barrier (the so-called “planar contact” limit). This value is approximately $1.31\Delta/e$, which is about 8% smaller than the Ambegaokar-Baratoff result for an insulating barrier. As the correlations increase, I_c decreases to be much below the bulk critical current of the junction, and R_n increases. The characteristic voltage has a rich behavior. For the thin junction ($N_b=1$) it is maximized in the correlated metallic regime, and becomes constant for the insulator. As the thickness increases to $N_b=2$, we continue to see a small maximum in the metallic regime, but the interesting behavior is that for a wide range of correlation strengths, the Ambegaokar-Baratoff result does not hold, and the characteristic voltage increases with correlation strength. For barrier thicknesses on the order of the correlation length ($N_b=5$), the behavior is even more complex. The voltage initially decreases with correlation strength, then has a sharp rise at the metal-insulator transition, followed by a maximum

for the correlated insulator that ultimately decreases as the correlations increase further. The Ambegaokar-Baratoff regime does not hold here either. Finally in the thick-junction regime ($N_b=20$), the resistance has a strong dependence on temperature in the insulating regime, and even at what is a low temperature for the superconducting properties, the characteristic voltage can decrease significantly as the correlations increase. The conclusion that can be drawn from this is that one requires a careful tuning of the thickness of the barrier, the proximity to the metal-insulator transition, and the operating temperature to optimize the properties of a junction. This idea is further supported in the next section.

IV. TUNING THE JUNCTION THICKNESS THROUGH THE METAL-INSULATOR TRANSITION

Here we present results on tuning the junction from the thin to thick barrier at three values of U_{FK} : (i) $U_{FK}=2$ a weakly correlated metal; (ii) $U_{FK}=4$ a strongly correlated (pseudogap) metal; and (iii) $U_{FK}=6$ a correlated insulator. In the correlated metal case, the junction can be viewed as a superconductor–normal-metal–superconductor (SNS) weak link,² while the correlated insulator barrier eventually leads to a superconductor-insulator-superconductor (SIS) junction. In the case with $U_{FK}=2$, the normal region is a non-Fermi liquid metal that can be described as dirty metal (resistivity $\rho_n \approx 240 \mu\Omega \text{ cm}$ with the assumption that the lattice constant is 3 \AA), for $U_{FK}=4$, we get a “bad metal” ($\rho_n \approx 2700 \mu\Omega \text{ cm}$; such huge resistivities do not necessarily require electronic correlations,³⁸ but are also seen in model calculations involving disordered Fermi liquids³⁹). The early experimental⁴⁰ and theoretical⁴¹ work on SNS junctions revealed that the supercurrent in these structures arises from the proximity effect: superconducting correlations are generated in the normal region with the density of pairs decreasing exponentially from the SN interface on a scale set by the normal metal coherence length $\xi_n = (\hbar D/2\pi k_B T)^{1/2}$ (here, D is a classical diffusion constant). The equilibrium current then flows at zero voltage because of the overlap of pair-field wave functions from the two superconductors. Recent mesoscopic advances have supplemented this “crude” picture with the analysis of energy-resolved quantities^{12,42} that become important for phenomena on small length scales at low temperatures and voltages.⁴³ The initial theoretical studies^{41,44} relied on Ginzburg-Landau theory (which formally requires T to be close to T_c) in the dirty limit ($\xi_0 \gg l$, with l the mean free path) and for long junctions ($N_b \gg \xi_n$).⁴¹ In the ensuing approaches, based on quasiclassical Green’s-function formalism, junctions with more general parameters were described,^{2,45} where the proximity effect on the superconducting side (i.e., a depression of the order parameter near the SN interface) was taken into account⁴⁶ (such effects are treated from the onset in self-consistent studies like ours). Thus, the conventional proximity-effect theories show that the critical current is determined primarily by the behavior of the superconducting order parameter when crossing a SN boundary, while its thickness dependence, and temperature dependence are affected by the way quantum coherence is lost in the normal metal. However, it is only recently that

mesoscopic studies⁴⁷ have emphasized the importance of the Thouless energy $E_{\text{Th}} = \hbar D / N_b^2 = 2\pi k_B T \xi_n^2 / N_b^2$ for the proximity effect.¹² Although E_{Th} is determined by the classical diffusion time N_b^2 / D for a particle to cross the sample, it plays a prominent role in various quantum phenomena encountered in disordered (normal) metal electron physics.⁴⁸ In the long junction limit $\Delta \gg E_{\text{Th}}$, the critical current is set by E_{Th} —according to the recent quasiclassical (non-self-consistent) calculations⁴⁷ $eI_c R_n(T=0) = 10.82 E_{\text{Th}}$. In the short junction limit $E_{\text{Th}} \gg \Delta$, for $T \rightarrow 0$, the product $I_c R_n$ is expected to be given by the diffusive limit $0.66\pi\Delta/e$ of the Kulik-Omelyanchuk formula,³³ or $1.92\Delta/e$ in the case of dirty interface with Schep-Bauer distribution of transparencies^{9,36} (as discussed in Sec. III). The high versus low-temperature limit is set⁴⁷ by the ratio of $k_B T$ and E_{Th} , or, equivalently, N_b and ξ_n , since $N_b = \xi_n$ is defined to be the length scale at which $k_B T = E_{\text{Th}}$.

While the energy gap Δ is determined by the (attractive) electron-electron interaction in the superconducting leads, E_{Th} is a single-electron concept, and as such is not directly applicable to our correlated metal (which has no well-defined Landau quasiparticles). Nevertheless, it is a common practice in experimental studies⁷ to extract estimates for such “quasiparticle” parameters⁷ using measured values of ρ_n , and check if the conventional treatment can describe the junction. We extract a diffusion constant D from the Einstein relation $1/\rho_n = 2e^2 N(E_F) D$ [with $N(E_F)$ the (single-spin) interacting density of states at the Fermi energy]. This is independent of band-structure effects (classically $D = v_F l / 3$, but D can also be defined quantum-mechanically from the Kubo formula in an exact state representation,³⁹ which then allows one to use a diffusivity even when the semiclassical picture of the mean-free path l breaks down). For the dirty-metal case $U_{FK} = 2$ we find $D_{U_{FK}=2} \approx 2ta^2/\hbar$ and for the bad-metal case we find $D_{U_{FK}=4} \approx 0.32ta^2/\hbar$. The corresponding normal metal coherence lengths are $\xi_n \approx 5.6a$ and $\xi_n \approx 2.3a$ (at $T = 0.01$) in the former and the latter case, respectively.

We calculate the critical current for ten thicknesses ranging from $N_b = 1$ to $N_b = 80$ (1, 2, 5, 10, 15, 20, 30, 40, 60, and 80) and fit to the following form:

$$I_c = AN_b^x \exp[-N_b / \xi_b], \quad (8)$$

with A a constant, ξ_b the coherence length in the barrier (the symbol ξ_b is used here to differentiate it from the phenomenological ξ_n determined from a diffusive metal analogy above), and x an exponent. We find that the fits vary from the analytic forms for the thick-barrier limit ($x = 1$). For example we find that the coherence length decreases from $\xi_b = 6.66$ for $U_{FK} = 2$, to $\xi_b = 2.96$ for $U_{FK} = 4$, to $\xi_b = 0.665$ for $U_{FK} = 6$. Similarly, the exponent varies from $x = -0.40$ for $U_{FK} = 2$, to $x = -0.45$ for $U_{FK} = 4$, to $x = -0.53$ for $U_{FK} = 6$. The value for the exponent never becomes close to the asymptotic result of $x = 1$ for a thick junction. But the coherence length behaves as expected—as the scattering increases, the coherence length decreases, becoming very small as the barrier goes through the metal-insulator transition and becomes a correlated insulator (in fact, our values

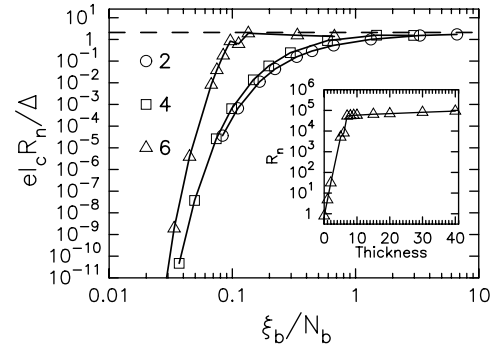


FIG. 12. Characteristic voltage plotted versus the inverse of the effective thickness of the barrier on a log-log plot. Using the correlation length extracted from the fit, allows us to plot the characteristic voltage against a measure of the Thouless energy $E_{\text{Th}} = 2\pi k_B T \xi_b^2 / N_b^2$. Such a plot should show scaling behavior, according to the quasiclassical theory; we find this to be approximately true for the metallic junctions ($U_{FK} = 2$, circles; and $U_{FK} = 4$, squares), but the correlated insulating barrier has a much sharper dependence on the barrier thickness (including an “oscillation”) and the scaling of the quasiclassical theory breaks down. Note the sharp onset of insulating behavior at a thickness $N_b \approx 7$ for $U_{FK} = 6$. Inset is the resistance versus barrier thickness for $U_{FK} = 6$. Note the sharp location of the metal-insulator transition near $N_b = 7$.

for ξ_b are only about 20% larger than the estimates for ξ_n given above). Note that this fitting procedure is not well defined, since we do not have data over many decades of barrier thicknesses and because we can trade off some effects of the fitting by simultaneously changing the exponent and the coherence length. But in all cases shown, we fit all of the data from $N_b = 5$ to $N_b = 80$ to an accuracy of better than 10% for the critical current (the accuracy decreases to about 25% for $N_b = 1$). This fitting scheme with nontrivial exponents is definitely more accurate than the best fits one can achieve with $x = 1$ or $x = 0$. We find the case with $U_{FK} = 4$ to be the toughest case to fit to this form (the spread in error is about 10% here, with 25% error for $N_b = 1$), while the $U_{FK} = 2$ case is the easiest, with a fit for all values $N_b = 1$ to 80 being accurate to 5%.

In Fig. 12, we plot the characteristic voltage (in units of Δ/e) versus the ratio of the barrier coherence length (determined from the fit of the critical current and equivalent to the Thouless length) to the barrier thickness. This is our analog of the recent results of a quasiclassical theory,⁴⁷ which show deviations of the Kulik-Omelyanchuk relation for long diffusive junctions. The results for metallic junctions $U_{FK} = 2, 4$, have the same shape as seen in the quasiclassical theory, and they nearly scale with each other (the scaling could be improved by slightly changing the barrier coherence length). The correlated-insulator results, $U_{FK} = 6$, however, show a different functional shape, with the transition from the nearly constant characteristic voltage to the region where it decreases sharply, occurring much more rapidly than in the metallic case (and having a small “oscillation” at the “transition”). One can be more quantitative in the comparison with the quasiclassical predictions: in the long-junction limit, the characteristic voltage is predicted⁴⁷ to behave like

$$I_c R_n = A' N_b^{x'} \exp[-N_b/\xi_b], \quad (9)$$

with the coherence length determined from the functional dependence of the critical current on N_b in Eq. (8). The quasiclassical prediction gives $A' \approx 5.49D/\xi_b^2$ and $x' = 1$. While we can fit reasonably well to this functional form in the regime where $\xi_b/N_b < 1$, we typically find the constant A' is about three to five times larger and the exponent x' is about a factor of 2 smaller than the quasiclassical predictions for the correlated metal cases ($U_{FK} = 2$ or 4). The parameters deviate significantly for the correlated-insulator phase (where the fitting breaks down severely for $\xi_b/N_b > 0.1$). *This shows that the correlated-insulator regime cannot be described by the conventional quasiclassical approach.* There appears to be a critical length at which point the characteristic voltage changes from an essentially constant dependence on the barrier thickness to a rapidly decreasing dependence on the thickness (which is $N_b \approx 7$ for $U_{FK} = 6$). The difference in shapes seen in Fig. 12 arises mainly from the behavior of the resistance, which assumes a linear scaling with the thickness N_b in the metallic regime and in the thick insulating regime (although it has an additional constant there, when extrapolated to $N_b = 0$), but has a rapid crossover to the linear regime for the thin insulator (semilogarithmic plot shown in the inset to Fig. 12).

One may wish to conclude from Fig. 12 that correlated insulating barriers are superior to metallic barriers since the parameter ξ_b/N_b can be reduced to much smaller values than in the metallic cases before the characteristic voltage becomes reduced. But such a view is erroneous, because the significantly smaller values of ξ_b for the insulating barriers means that the barrier thicknesses where the characteristic voltage starts to decrease are indeed smaller for the correlated insulator. What can be inferred from the figure, however, is that once one reaches the critical thickness where the barrier has a metal-insulator “transition,” the characteristic voltage is very strongly dependent on the thickness of the junction. Hence variations in the thickness of the barrier can have a large effect on the performance of a junction with a correlated-insulator barrier. In particular, variations in the thickness could make junctions appear to have “pinholes” because slightly thinner areas can have greatly enhanced Josephson coupling. This can possibly explain why it appears to be more difficult to attain small spreads in junction properties for high- T_c -based junctions, even if the barrier is free of conventional pinholes because the proximity to the thickness triggered metal-insulator transition generates “intrinsic pinholes” within the correlated insulator.

It is also interesting to examine how the anomalous average behaves as a function of the thickness of the barrier as well. We find the following result shown for $U_{FK} = 4$ in Fig. 13: once the thickness is larger than the bulk coherence length (i.e., for all barriers simulated with $N_b \geq 5$), we find that the shape of the anomalous average is identical for all thicknesses for the planes that lie within the superconducting region and that penetrate two to three planes into the barrier. What this tells us is that the thickness of the barrier is not influencing the shape of the anomalous average except within the barrier itself, so the oscillations are a property of

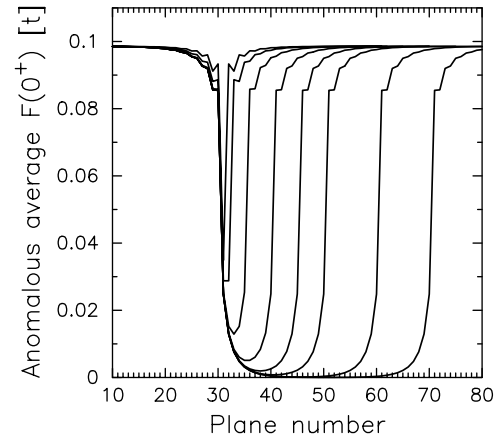


FIG. 13. Anomalous average versus plane number for ($U_{FK} = 4$) and thicknesses ranging from $N_b = 1, 2, 5, 10, 15, 20, 30,$ and 40 (the thickness of each barrier is obvious from the range of the plots). Note how the shapes of these curves are identical for the regions close to the superconductor-barrier interface at planes 25–34 (and within the superconducting region to the right or the left for the right or left interface, respectively). Since this shape stops changing after $N_b = 2$, we conclude that the oscillations are an intrinsic property of the bulk superconductor terminated on the barrier.

the bulk superconductor coming in contact with the barrier. These results are also true for the $U_{FK} = 2$ and $U_{FK} = 6$ cases, but we do not show those results here, because the agreement is essentially the same as seen in the $U_{FK} = 4$ figure below.

V. CONCLUSIONS

In this work we have examined what happens as the barrier of a junction is tuned from a metal to an insulator for short coherence-length s -wave superconductors. We studied the transition both as a function of the correlation strength and of the barrier thickness. We found a number of interesting results. First, in regimes where the critical current density approaches that of the bulk superconductor, self-consistency is important in determining the current-phase relation, and it is modified dramatically from simple sinusoidal behavior. As the correlations increase, and the current density decreases, the sinusoidal behavior is restored, but in some cases, the maximum of the current-phase curve overshoots $\pi/2$ and then becomes sinusoidal only at an even larger correlation strength. Second, we found that as the barrier becomes more insulating, the anomalous pair-field average develops oscillations on the order of the Fermi wavelength, which can be quite substantial in amplitude (up to about twice the bulk anomalous average). These oscillations are tied to the superconductor-insulator interface, and depend little on the thickness of the barrier once the thickness is larger than about twice the bulk coherence length. Third, we found that the critical current has a nontrivial dependence on the thickness of the barrier—while it decays exponentially with thickness, it also has a power-law prefactor that varies with correlation strength, and deviates sharply from the quasiclassical prediction. The barrier coherence length de-

creases, of course, as the correlation strength increases into the insulating regime. Fourth, we found that the characteristic voltage has rich behavior. It is maximized for weakly correlated metallic barriers for thin junctions and the Ambegaokar-Baratoff result is recovered at strong correlations. As the barrier thickness increases, the maximum in the metallic region is reduced, but the Ambegaokar-Baratoff result fails as the correlations increase, with the characteristic voltage increasing linearly with U_{FK} over a wide range of correlation strengths. The intermediate thickness junctions have the most interesting behavior—the voltage initially decreases, has a sharp increase at the metal-insulator transition, and then decreases in the large correlation limit. Thick insulating barriers have very low characteristic voltages and strong temperature dependence, as expected at finite temperatures, since the junction resistance decreases rapidly as the temperature is increased in the insulating regime. We also saw that self-consistency can renormalize the Ambegaokar-Baratoff limit, reducing it by about 10% for the single-plane barrier. Fifth, we saw a dramatic deviation from the quasi-classical predictions as the barrier becomes insulating due to strong electron correlations. The characteristic voltage remains high for a larger range of Thouless energy than in metallic junctions, and then decreases very rapidly as the barrier passes through a critical thickness where the metal-insulator transition occurs. This behavior leads to the possibility of “intrinsic pinholes.”

This work shows that correlation effects, and the interplay

between superconductivity and oscillations brought on by the underlying Fermi surface, play increasingly important roles in short-coherence-length superconductors. In particular, optimizing the characteristic voltage of a junction near the metal-insulator transition is possible, but requires a careful tuning of the thickness of the barrier, the proximity to the metal-insulator transition, and the operating temperature of the device. Correlated insulating barriers can mimic effects due to pinholes because the Josephson coupling depends very strongly on the thickness leading to an “intrinsic” pinhole effect. In the future, we plan on extending this work to d -wave superconductors for direct applications to high- T_c superconductors.

ACKNOWLEDGMENTS

We are grateful to the Office of Naval Research for funding under Grant No. N00014-99-1-0328. Real-axis analytic continuation calculations were partially supported by the National Computational Science Alliance under Grant No. DMR990007N (utilizing the NCSA SGI/CRAY ORIGIN 2000) and were partially supported by a grant of HPC time from the Arctic Region Supercomputer Center. We wish to acknowledge useful discussions with T. Van Duzer, J. Ketterson, T. Klapwijk, J. Luine, J. Mannhart, I. Nevirkovets, N. Newman, J. Rowell, and S. Tolpygo. J.K.F. thanks the hospitality of the IBM, Almaden Research Center, where this work was completed.

-
- ¹B. D. Josephson, Phys. Lett. **1**, 251 (1962).
²K. K. Likharev, Rev. Mod. Phys. **51**, 101 (1979).
³For a recent review see the special issue of Superlattices Microstruct. **25**, No. 5/6 (1999).
⁴A. Kastalskii, A. W. Kleinsasser, L. H. Greene, R. Bhat, F. P. Milliken, and J. P. Harvison, Phys. Rev. Lett. **67**, 3026 (1991); V. T. Petrashov and V. N. Antonov, Pis'ma Zh. Eksp. Teor. Fiz. **54**, 245 (1991) [JETP Lett. **54**, 241 (1991)].
⁵C. W. J. Beenakker, Rev. Mod. Phys. **69**, 731 (1997).
⁶C. J. Lambert and R. Raimondi, J. Phys.: Condens. Matter **10**, 901 (1998).
⁷K. A. Delin and A. W. Kleinsasser, Supercond. Sci. Technol. **9**, 227 (1996); R. S. Decca, H. D. Drew, E. Osquiguil, B. Maiorov, and J. Guimpel, Phys. Rev. Lett. **85**, 3708 (2000).
⁸A. S. Barrera and M. R. Beasley, IEEE Trans. Magn. **MAG-23**, 866 (1987).
⁹A. Bardas and D. V. Averin, Phys. Rev. B **56**, R8518 (1997).
¹⁰A. Levy Yeyati, A. Martín-Rodero, and F. J. García-Vidal, Phys. Rev. B **51**, 3743 (1995).
¹¹J. C. Cuevas, A. Martín-Rodero, and A. Levy-Yeyati, Phys. Rev. B **54**, 7366 (1996).
¹²W. Belzig, F. K. Wilhelm, C. Bruder, G. Schön, and A. D. Zaikin, Superlattices Microstruct. **25**, 1251 (1999).
¹³J. Rammer and H. Smith, Rev. Mod. Phys. **58**, 323 (1986).
¹⁴S.-K. Yip, Superlattices Microstruct. **25**, 1213 (1999).
¹⁵W. Metzner and D. Vollhardt, Phys. Rev. Lett. **62**, 324 (1989).
¹⁶M. Potthoff and W. Nolting, Phys. Rev. B **59**, 2549 (1999).
¹⁷P. Miller and J. K. Freericks, J. Phys.: Condens. Matter **13**, 3187 (2001).
¹⁸L. M. Falicov and J. C. Kimball, Phys. Rev. Lett. **22**, 997 (1969).
¹⁹J. Hubbard, Proc. R. Soc. London, Ser. A **276**, 238 (1963).
²⁰F. Sols and J. Ferrer, Phys. Rev. B **49**, 15 913 (1994).
²¹Li-Fu Chang, S. Chaudhuri, and P. F. Bagwell, Phys. Rev. B **54**, 9399 (1996).
²²N. Agrait, J. G. Rodrigo, C. Sirvent, and S. Vieira, Phys. Rev. B **46**, R5814 (1992).
²³J. Bardeen, L. Cooper, and J. Schrieffer, Phys. Rev. **108**, 1175 (1957).
²⁴P. G. de Gennes, *Superconductivity of Metals and Alloys* (Addison-Wesley, Redwood City, CA, 1966).
²⁵P. Nozières and S. Schmitt-Rink, J. Low Temp. Phys. **59**, 195 (1985).
²⁶M. Keller, W. Metzner, and U. Schollwöck, Phys. Rev. Lett. **86**, 4612 (2001).
²⁷A. J. Legget, in *Modern Trends in the Theory of Condensed Matter*, edited by A. Pekalski and J. Przystawa (Springer, Berlin, 1980).
²⁸P. G. J. van Dongen, Phys. Rev. B **45**, 2267 (1992); P. G. J. van Dongen and C. Leinung, Ann. Phys. (Leipzig) **6**, 45 (1997).
²⁹J. Bardeen, Rev. Mod. Phys. **34**, 667 (1962).
³⁰Y. Nambu, Phys. Rev. **117**, 648 (1960).
³¹E. N. Economou, *Green's Functions in Quantum Physics*, (Springer-Verlag, Berlin, 1983), Appendix B.
³²A. Khurana, Phys. Rev. Lett. **64**, 1990 (1990).

- ³³I. O. Kulik and A. N. Omelyanchuk, *Fiz. Nizk. Temp.* **3**, 945 (1977) [*Sov. J. Low Temp. Phys.* **3**, 459 (1977)].
- ³⁴O. N. Dorokhov, *Pis'ma Zh. Éksp. Teor. Fiz.* **36**, 359 (1982) [*JETP Lett.* **36**, 318 (1982)].
- ³⁵K. M. Schep and G. E. W. Bauer, *Phys. Rev. Lett.* **78**, 3015 (1997).
- ³⁶Y. Naveh, V. Patel, D. V. Averin, K. K. Likharev, and J. E. Lukens, *Phys. Rev. Lett.* **85**, 5404 (2000).
- ³⁷V. Ambegaokar and A. Baratoff, *Phys. Rev. Lett.* **10**, 486 (1963).
- ³⁸O. Gunnarsson and J. E. Han, *Nature (London)* **405**, 1027 (2000).
- ³⁹B. K. Nikolić and P. B. Allen, *Phys. Rev. B* **63**, 020201(R) (2001).
- ⁴⁰J. Clarke, *Proc. R. Soc. London, Ser. A* **308**, 447 (1969); J.G. Shepherd, *ibid.* **326**, 421 (1969).
- ⁴¹P. G. de Gennes, *Rev. Mod. Phys.* **36**, 225 (1964).
- ⁴²S.-K. Yip, *Phys. Rev. B* **58**, 5803 (1998).
- ⁴³H. Curtois, Ph. Gandit, D. Maily, and B. Pannetier, *Phys. Rev. Lett.* **76**, 130 (1996).
- ⁴⁴H. J. Fink, *Phys. Rev. B* **14**, 1028 (1976).
- ⁴⁵A. D. Zaikin and G. F. Zharkov, *Fiz. Nizk. Temp.* **7**, 385 (1981) [*Sov. J. Low Temp. Phys.* **7**, 184 (1981)].
- ⁴⁶M. Yu. Kupriyanov and V. Lukichev, *Fiz. Nizk. Temp.* **8**, 1045 (1982) [*Sov. J. Low Temp. Phys.* **8**, 526 (1982)].
- ⁴⁷P. Dubos, H. Courtois, F. K. Wilhelm, A. D. Zaikin, and G. Schön, *Phys. Rev. B* **63**, 064502 (2001).
- ⁴⁸M. Janssen, *Phys. Rep.* **295**, 1 (1998).